Research Journal of Environmental Sciences

ISSN 1819-3412

Academic
Journals Inc.

www.academicjournals.com

OPEN ACCESS Research Journal of Environmental Sciences

ISSN 1819-3412
DOI: 10.3923/rjes.2017.82.93

Research Article
2DV Regular Plunging Breaking Waves in the Surf Zone

Evangelos Koutandos

Institute of Marine Biology, Biotechnology and Aquaculture, Hellenic Centre for Marine Research, Thalassocosmos, P.O.Box 2214, GR-71003 Heraklion, Crete, Greece

Abstract

Background and Objective: Wave breaking in the coastal region is one of the most important hydrodynamic quantities in terms of the beach morphology, sediment transport and wave energy dissipation. Due to the significant coastal impact, wave breaking has been the focus of environmental sciences and especially environmental engineering for decades. When the incident wave train impinges on the inclined beach, part of the energy is reflected back to the sea and a part is dissipated. Most of the incident wave energy is lost essentially by breaking. These nonlinearities are of paramount importance for understanding sediment dynamics. Therefore in this study understand about relative contribution that is of paramount importance to better grasp how is nearshore morphodynamics driven. **Materials and Methods:** An experimental study was conducted in the CIEM flume of the Catalonia University of Technology, Barcelona. Regular waves trains of various heights and periods were generated for plunging breaking conditions in order to study the wave hydrodynamics in the surf zone. A 2DV numerical study was also conducted using the cornell breaking waves and structure (COBRAS) model in order to present the 2DV hydrodynamic characteristics, velocity, turbulent kinetic energy, of regular, plunging breaking waves in the surf zone. **Results:** According to the analysis of this study, during wave breaking, the velocity of fluid particles at the wavefront and the region near the free surface precedes the wave speed. Velocity has its maximum value at the upper part, where the surface roller occurs, very close to the free surface, under the wave crest. Maximum turbulent kinetic energy and dissipation rate are located below the wave crest and near the free surface at breaking time. **Conclusion:** Significant non-linear interactions occur in the surf zone and some energy is transferred from the fundamental wave frequency to higher harmonics. A significant portion of turbulence dissipation occurs at the high-frequency tail (Kolmogorov scale) and energy can be definitely transferred and subsequently absorbed at higher frequencies than the wave harmonics.

Key words: Breaking waves, plunging waves, surf zone, spectral analysis, wave energy transfer

Citation: Evangelos Koutandos, 2017. 2DV regular plunging breaking waves in the surf zone. Res. J. Environ. Sci., 11: 82-93.

Corresponding Author: Evangelos Koutandos, Institute of Marine Biology, Biotechnology and Aquaculture, Hellenic Centre for Marine Research, Thalassocosmos, P.O.Box 2214, GR-71003 Heraklion, Crete, Greece Tel: 2810337779

Competing Interest: The author has declared that no competing interest exists.

Data Availability: All relevant data are within the paper and its supporting information files.

INTRODUCTION

Surf zone breaking waves influence most coastal morphology processes. These waves produce highly turbulent regions causing significant mixing and sediment suspension. The suspended sediments are transported by the nearshore currents induced by breaking waves. Investigations of surf zone hydrodynamics entail field experiments, laboratory measurements and models.

Although, laboratory measurements have some limitations, due to the constrained circumstances compared with the field, the data obtained are the most reliable for investigating processes and for validating models. Meanwhile, developments in computational hardware and numerical solution methods have driven the popularity of numerical modeling of coastal hydrodynamics. Three major classes of numerical models in the nearshore zone have been utilized, namely, shallow water equations, Boussinesq-type models and Navier–Stokes (NS) solvers[1-3]. Computational limitations have limited most modeling efforts to depth-averaged equations, such as those based on the shallow water equation and the Boussinesq assumption. Although, these formulations have generally performed well, the depth-averaged formulation does not yield the detailed internal flow structure necessary for applications such as the prediction of sediment transport in the swash zone.

Various approaches have been presented for modeling vertical motion within waves. To better simulate the flow and turbulence fields at the time of wave breaking, all hydrodynamic governing equations should be investigated. In principle, direct numerical simulation (DNS) can be implemented for the simulation of wave breaking[4]. For high Reynolds number turbulent flows, numerical simulations of the turbulence oscillations require very fine time steps and are therefore computationally demanding. In general, computational demands are high for DNS methods. Another framework for numerical simulation of wave breaking is the implementation of models based on the Reynolds-Averaged Navier–Stokes (RANS) equations. Here, the average motion of flow is described and the effects of turbulent oscillations on the average flow are considered by the Reynolds stresses. In order to compute the Reynolds stresses and the turbulence characteristics, turbulence closure models are used. Examples of such models are those in applied the standard k-ϵ model to simulate breaking waves in the surf zone and their impact on coastal structures in that zone[3]. The k-ϵ turbulence model, which is related to the turbulent energy k and the rate of energy dissipation ϵ, models the spatially and temporally varying eddy viscosity. Bradford [5] compared the performance of the k model, linear k-ϵ model and a renormalized group extension of the k-ϵ model in the surf zone. It was found that all these models predict wave breaking far earlier than that observed in experiments, while also underestimating the undertows. Instead of the k-ϵ model, other investigators have used large eddy simulation (LES) for describing the eddy viscosity in the nearshore zone[6]. Zhao *et al.*[7], used the multi-scale turbulence model to simulate breaking waves. The turbulence level near the breaking point was too high. Christensen[6] extended an LES model that described hydrodynamics in the surf zone. This model encompasses the NS equations, the free surface model and the subgrid scale model (SGS). A hydrodynamic model has been combined with a free surface model based on the surface markers method to simulate the flow field in breaking waves, where the large turbulent eddies have been simulated by the LES method and the small scale turbulence is represented by a simple smagorinsky sub-scale model.

It is important to note that most models based on a two-equation k-ϵ turbulence model make use of nearly the same values for the empirical constants contained within it. This model is used frequently and so its application to modeling of the hydrodynamics of the combined surf and swash zones would be, if successful, a valuable addition to its range of applications. Since the RANS model can describe both the mean velocity and turbulence fields, it is expected that would reliably model surf zone dynamics, especially for the time averaged mean flow. The latter is important as, for example, accurate information on it, is essential for predicting sediment transport in the nearshore zone. The influence of all these processes on water motion and sediment transport varies significantly along the cross-shore beach profile and it is the understanding of these relative contributions that is of paramount importance to better grasp how is nearshore morphodynamics driven.

MATERIALS AND METHODS

In this study, hydrodynamic processes in the surf zone are investigated under regular, plunging breaking wave trains action. For this purpose, a combination of a two-dimensional RANS solver with a k-ϵ turbulence model (COBRAS wave model) with experimental results is presented. Laboratory measurements analysis and numerical simulations were performed in Institute of Marine Biology, Biotechnology and Aquaculture, in Hellenic Centre for Marine Research, in 2014.

Experimental facility and procedure: The experiments were conducted in the CIEM flume of LIM at UPC in Barcelona.

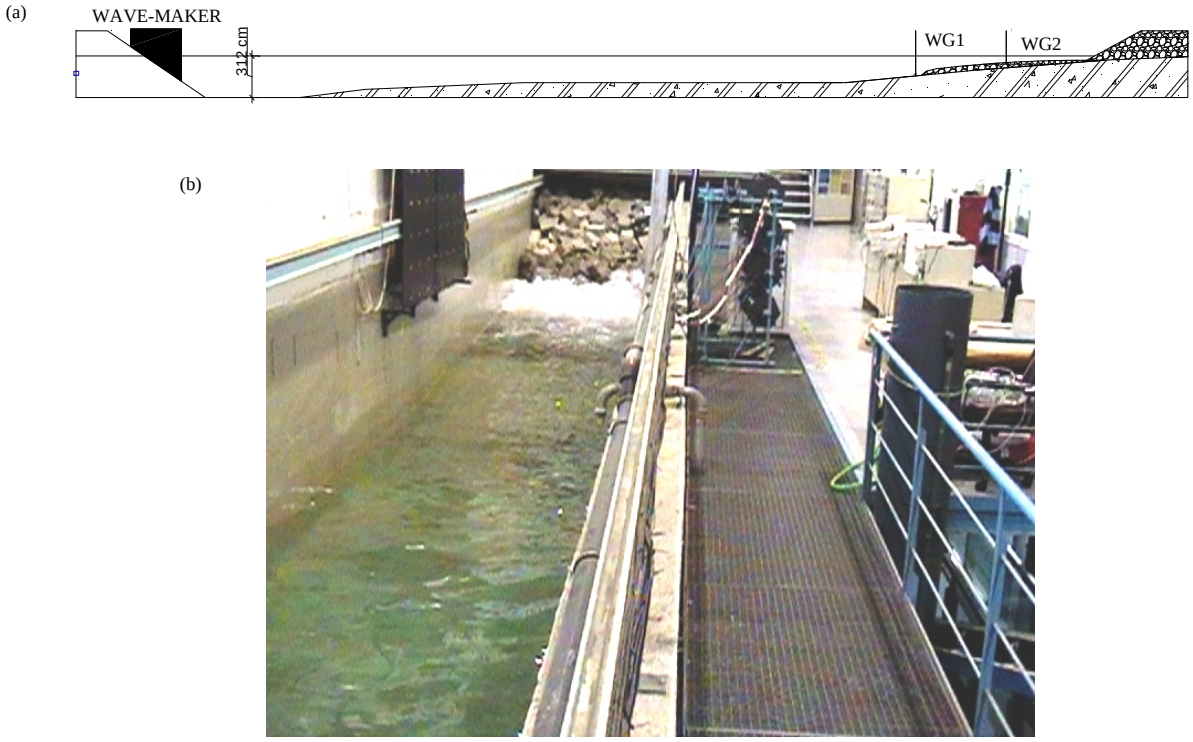

Fig. 1(a-b): (a) Layout of the flume and the instrumentation and (b) General view of the experimental flume

Table 1: Regular wave test conditions

	T (sec)	H (cm)	ξ
R1	2.80	0.20	0.69
R2	4.00	0.10	1.39
R3	4.00	0.30	0.80
R4	4.00	0.50	0.62
R5	6.00	0.15	1.70
R6	6.00	0.25	1.32
R7	6.00	0.40	1.04

ξ: Iribarren number

Regular waves trains of various heights and periods were generated for plunging breaking conditions according to Table 1, in order to study wave hydrodynamics in the surf zone.

An HR Wallingford wedge-type, wave maker was used, while the experimental equipment consisted of two Wallingford wave gauges in the surf zone. The layout of the flume and the instrumentation are presented in Fig. 1(a-b). The sampling frequency during the experiments was 20 Hz. Seven regular wave trains were generated with various wave heights and periods according to Table 1, for plunging breaking conditions.

Description of the numerical model: In the COBRAS wave model the Reynolds Averaged Navier-Stokes (RANS) equations are solved in a 2DV computational field[3]. Turbulence closure is achieved using a non-linear k-ϵ type turbulence model. Free surface evolution is described using the VOF method[8]. Porous medium are also included in the model. Direct numerical simulation in the porous medium is practically impossible due to the random geometry of the porous structure. Therefore the flow in the porous medium must be described using an integrated form of the Navier-Stokes over a certain control volume (Volume-Averaged Reynolds Averaged Navier-Stokes-VARANS). This control volume is larger than the pore structure but smaller than the characteristic length of the flow[9]. Another set of k-ϵ equations similar to the previous one is used to model turbulence production dissipation within the porous media.

The boundary conditions of the mean flow field consist of a non-slip condition at the solid boundaries and a zero stress condition at the free-surface[8]. With respect to the turbulence field, a log-law distribution of the mean tangential velocity in the turbulent boundary layer is considered near the solid boundary, where the values of k and ϵ can be expressed as functions of the distance from the solid from the solid boundary and the mean tangential velocity outside the viscous sublayer. On the free surface, the zero gradient boundary conditions for both k and ϵ are based on the

assumption of no turbulence exchange between the air and water. The initial condition consists of a still water situation. The wave model includes a procedure of wave generation using an internal wave maker. The method consists of introducing a source function in the continuity equation for a group of cells defining the source region. The free surface above the source region responds to a pressure increment defined within the source region cells and a train of surface gravity waves is generated[10]. A sponge-layer method[11], is used to absorb the waves that propagate in the direction opposite the zone of interest, with an imposed exponential damping law.

The computational domain in the wave model is discretized in rectangular cells. The computing mesh can be divided into submesh regions, which allows a variable cells spacing: A finer grid can be defined for the representation of specific study zones. The free surface is tracked using the volume of fluid (VOF) method developed by Hirt and Nichols[8] that identifies the free surface location, tracking the density change in each cell. Besides, the model allows the definition of flow obstacles using a partial cell treatment. The Reynolds equations are solved using a finite differences two-step projection method[12].

Governing equations: The RANS equations that describe the flow in the region outside the porous structure are the classical continuity and momentum equation[3].

The VARANS equations that describe the flow in the porous medium are the following[9].

Continuity Equation:

$$\frac{\partial < U_i >}{\partial x_i} = 0 \tag{1}$$

Momentum equation:

$$(1+C_A)\frac{\partial \langle U_i \rangle}{\partial t} + < U_j > \frac{\partial \langle U_i \rangle}{\partial x_j} = \left[-\frac{1}{\rho}\frac{\partial \langle P \rangle}{\partial x_i} - \frac{\partial \langle \mu_i \mu_j \rangle}{\partial x_j} + \frac{1}{\partial}\frac{\partial \langle \tau_{ij} \rangle}{\partial x_j} + g_i \right] - \left[a_1 \langle U_i \rangle + a_2 \left(< U_j >< U_j > \right)^{1/2} \langle U_i \rangle \right] \tag{2}$$

where the capitals letters denote the ensemble average and the non capitals represent turbulent fluctuations with respect to the ensemble mean. The Darcy's volume averaging operator, <>, is defined as $\langle a \rangle = \frac{1}{V}\int_{Vf} adV$ where V denotes the total averaging volume and V_f is the portion of V that is occupied by the fluid, which differs from the intrinsic averaging operator ,<>^{f}, defined by $\langle a \rangle^f = \frac{1}{V_f}\int_{Vf} adV$. The relationship between the Darcy's volume averaging and intrinsic volume averaging is $\langle a \rangle = n\langle a \rangle^f$ where n is the porosity $(n = V_f / V)$. C_A denotes the added mass coefficient $\left(C_A = \gamma_p (1-n)/n, \gamma_p = 0.34\right)$ and n is the porosity. The last two terms in equation (2) are known as Darcy and Forchheimer terms, respectively.

Coefficients a_1 and a_2 are calculated from the following relationships[13]

$$a_1 = \frac{v}{K}, a_2 = \frac{C_f}{\sqrt{K}} \tag{3}$$

where v is the water kinematic viscosity ($1.0 \cdot 10^{-6}$ m^2 sec^{-1}), C_f a dimensionless coefficient and K the permeabitlity (m^2) provided by the following[14]:

$$K = \frac{D_{50}^2 . n^3}{\alpha (1-n)^2} \tag{4}$$

where D_{50} is the mean diameter of the porous material and α an empirical coefficient.

According to Van Gent[14], for the calculation of C_f (Eq. 3) the following relationship is proposed:

$$C_f = \beta \frac{1-n}{n}\frac{\sqrt{K}}{D_{50}} \tag{5}$$

where β is an empirical coefficient.

In the regions outside the porous material where n = 1 and $C_A = 0$ the VARANS equations return to the original RANS equations.

Numerical simulations: The type of wave breaking and surf zone hydrodynamics are characterized by the Iribarren number, $\xi = \frac{\tan(a)}{\sqrt{\frac{Ho}{Lo}}}$, where a is the bed slope while Ho and Lo are, respectively, the height and length of waves in deep water. When ξ <0.5, the breaking zone is saturated and spilling breakers occur. For ξ > 0.5 the conditions are unsaturated and plunging breakers occur. Plunging breaking conditions are used for the investigation of surf zone hydrodynamics, according to Table 1.

Seven regular wave trains were generated with various wave heights and periods were generated, according to Table 1, for plunging breaking conditions, in order to study wave hydrodynamics in the surf zone.

Several grids have been employed to test the grid dependency of the results. It is found that the same results are obtained for the water surface elevation and the velocity field even if a coarser grid is used. This is not the case for the turbulent quantities for which the grid dependency is stronger. For the grid employed (2000×125) the results for both the mean and the turbulence quantities are considered grid independent. The time-step used in the computation is 0.005 sec about 8 times less than the Courant number limited time-step for reasons of accuracy, leading to time consuming numerical tests. The total computational time for these tests was taken 40 T and the results presented are from 30 T for which numerical stability is achieved, indicated by the total mass and energy in the domain.

RESULTS AND DISCUSSION

Flow field: Before the wave reaches the slope, the wave profile is symmetric. However, when the wave propagates along the slope, due to shoaling the wave symmetry vanishes. The upper sections of the wave proceed faster than the other parts so that the slope at the wave front gradually increases. Before breaking, the velocity field is non rotational except for the regions adjacent to the bed and the free surface. In shallow water the wave touches the bottom and begins to shoal. This affects the oscillatory motion of the water and causes the orbital wave motion to become distorted. Drag and bottom friction cause the spherical orbit of the oscillating wave to transform first to an elliptical orbit and then ultimately to collapse causing the wave to break[15].

A comparison between experimental and numerical results concerning the free surface elevation in WG1 and WG2, in the outer and in the inner region of breaking in the surf zone, for R7 (T = 4.00 s and H_i = 0.40 m) is presented, as shown in Fig. 2. The wave model describes satisfactorily wave breaking and the non linear phenomena appearing in free surface elevation.

Snapshots of distribution of velocities in the area near the breaking point are illustrated in Fig. 3 and 4. As seen from these figures, the region with the highest velocity is located ahead of the wave crest, at the wave front. Velocity has a maximum value at the upper part, where the roller occurs, near the free surface, under the wave crest[16-20]. After wave breaking, some vortices are generated in the surf zone starting from the breaking point and then convected to deeper areas. A breaking wave typically produces horizontal rollers, featuring two-dimensional rotational motion along the wave direction[21-23]. These vortices are expected to dissipate the energy of the incident wave. At the upper part, the water also

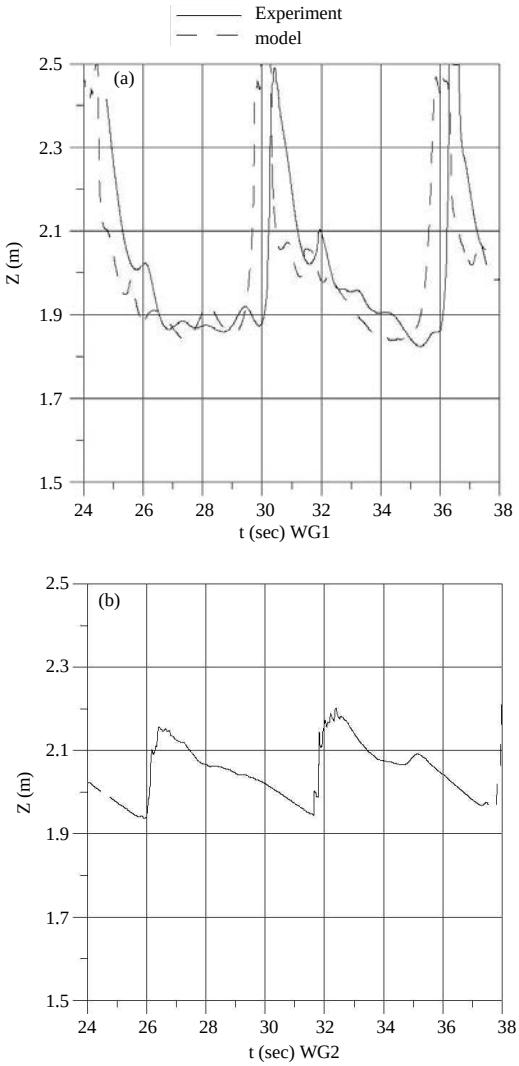

Fig. 2: Free surface elevation in WG1 and WG2 for T = 4.00 s and H_i = 0.40 m (experiment and model)

tends to move shoreward, which is balanced at the lower part where the water tends to move offshore.

Furthermore, the numerical results show that convective accelerations and Reynolds stresses are the main controls on horizontal velocity immediately after breaking.

Turbulence field: Turbulence transformations in the regions near the coast play an important role in beach morphodynamics, including sediment transport. The turbulence dynamics are known to be different in plunging and spilling breakers. Hence, it is expected that the effects of plunging and spilling breakers in the surf zone on the sediment transport and as a result, the erosion and accretion, is different.

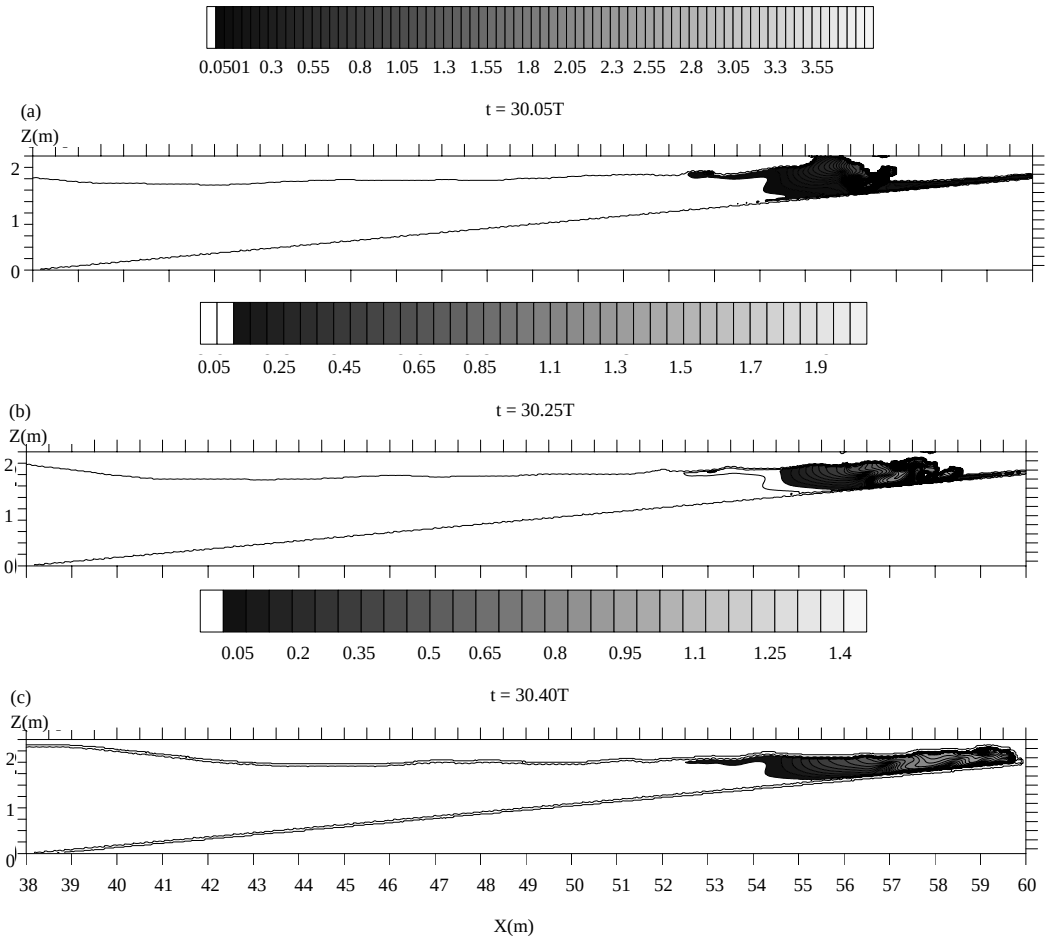

Fig. 3(a-c): Velocity field (T = 4.00 s, H_i = 0.40 m) for (a) t = 30.05T, (b) 30.25T and (c) 30.40T

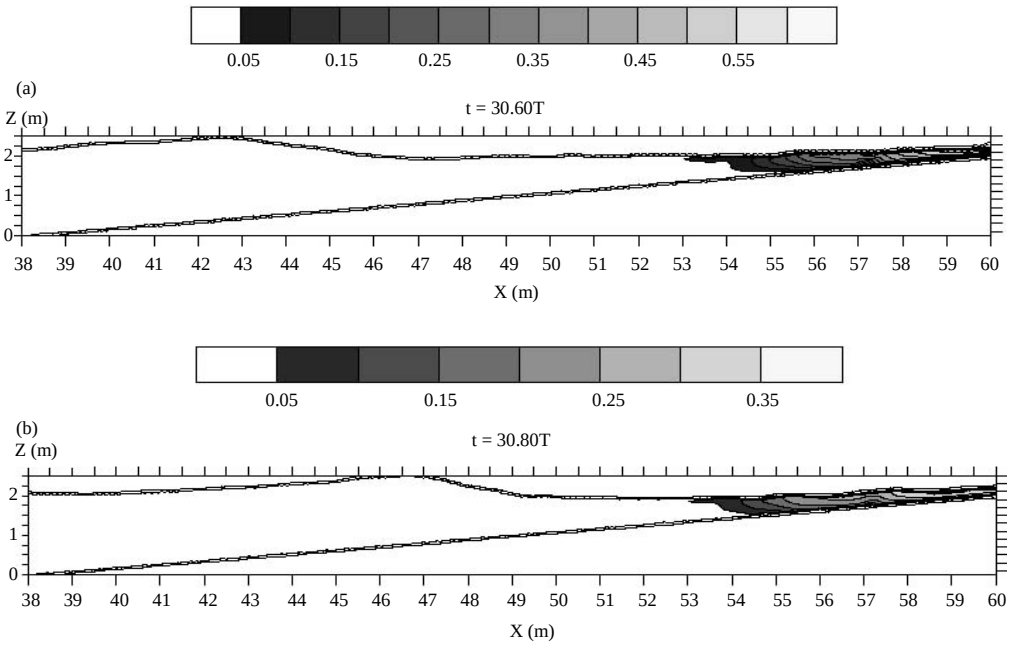

Fig. 4(a-c): Continue

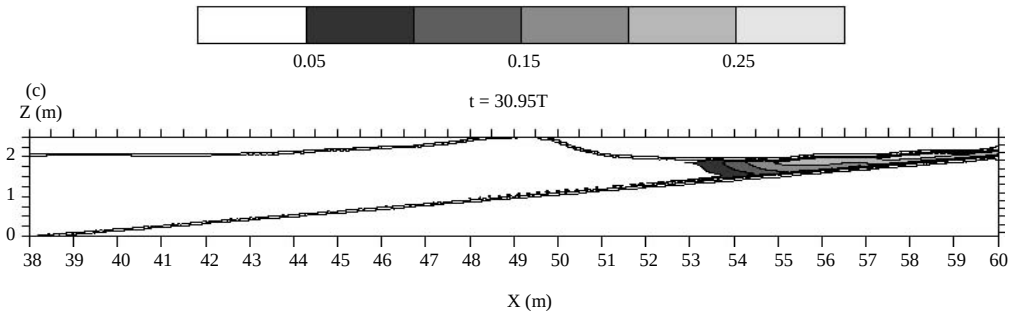

Fig. 4(a-c): Velocity field (T = 4.00 s, H_i = 0.40 m) for (a) t = 30.60T, (b) 30.80T and (c) 30.95T

Snapshots of distribution of the turbulence kinetic energy, which is presented through mean velocity fluctuation $\left(\sqrt{2k}\right)$, in the area near the breaking point are illustrated in Fig. 5 and 6. The maximum turbulent energy occurs under the wave crest, behind the wave front and near the free surface. The turbulence generated in the surface roller is rapidly transported to the depths of the flow and the rear regions of the wave front by the turbulence transformation mechanisms. In this region rotational motions occur and there is mixing of water and air. This complexity is difficult to describe accurately. The turbulence kinetic energy, is concentrated under the wave crest and behind the wave front. Another notable aspect is that the turbulence is more distributed horizontally in the flow direction rather than vertically. In plunging breakers advection is dominant in the propagation of turbulence, whereas in spilling breakers the turbulence distribution is mostly caused by turbulent diffusion. In the case of a plunging breaker, the time variation of turbulence is very high. Throughout the breaking, a large amount of turbulence is rapidly generated and then quickly dissipated[24-29]. After wave breaking, turbulent velocity fluctuations increase in the onshore direction. Numerical results show that turbulent velocities decrease with distance from the surface. These results are not consistent with the common assumption that in the surf zone the turbulence mechanism is breaker-generated turbulence in the proximity of the surface rollers. The turbulence generated by the wave-induced flow itself, is weak and therefore turbulent energy below the trough level is largely due to spreading of turbulence from the surface toward the bottom. Under the plunging breaker turbulence levels are higher and vertical variations of turbulent intensity and undertow are smaller in comparison with the spilling breaker. The velocity and turbulent variations before, at and after wave breaking are important hydrodynamic characteristics. During wave breaking all turbulence processes near the free surface are considerably more severe than the turbulence near the bed. In other words, the maximum rate of turbulent dissipation occurs under the wave crest near the free surface, in regions close to the wave front and below the wave crest[24-29].

While the sources of turbulence are approximately understood, a comprehensive description of the turbulence details is in the preliminary stages. This is likely due to the fact that wave breaking induces high curvature and consequently strong vorticity that is 3-D. Watanabe *et al.*[21], investigated the vortices in breaking waves and discovered the existence of "plural horizontal vortices", parallel to the wave front and oblique descending eddies, aligned to the principal axis of velocity deformation. Thus, for improving the prediction of turbulent characteristics in the breaking area, we need to extend the models to 3-D. The numerical resolution of high Reynolds number turbulent flows (such as wave breaking) demands very small time steps, which is computationally intensive.

Energy transfer: Wave spectra in WG1 and WG2, in the outer and in the inner region of breaking in the surf zone, for R7 (T = 4.00 s and H_i = 0.40 m) are presented in Fig. 7 and 8. Significant non-linear interactions occur in the surf zone and some energy is transferred from the fundamental wave frequency to higher harmonics. Spectrums undergo significant changes under the combined effects on non-linear energy transfer and dissipation. Spectra in the outer and in the inner region of breaking verify the intense energy decay. In WG1, in the outer region of breaking, we observe that the wave develops up to 3rd order harmonics while in WG2, in the inner region of breaking, it develops up to 5th order harmonics. Max spectral density value in WG1 spectrum is 1, while due to energy decay and spreading, max spectral density value in WG2 spectrum is 0.56. A significant portion of turbulence

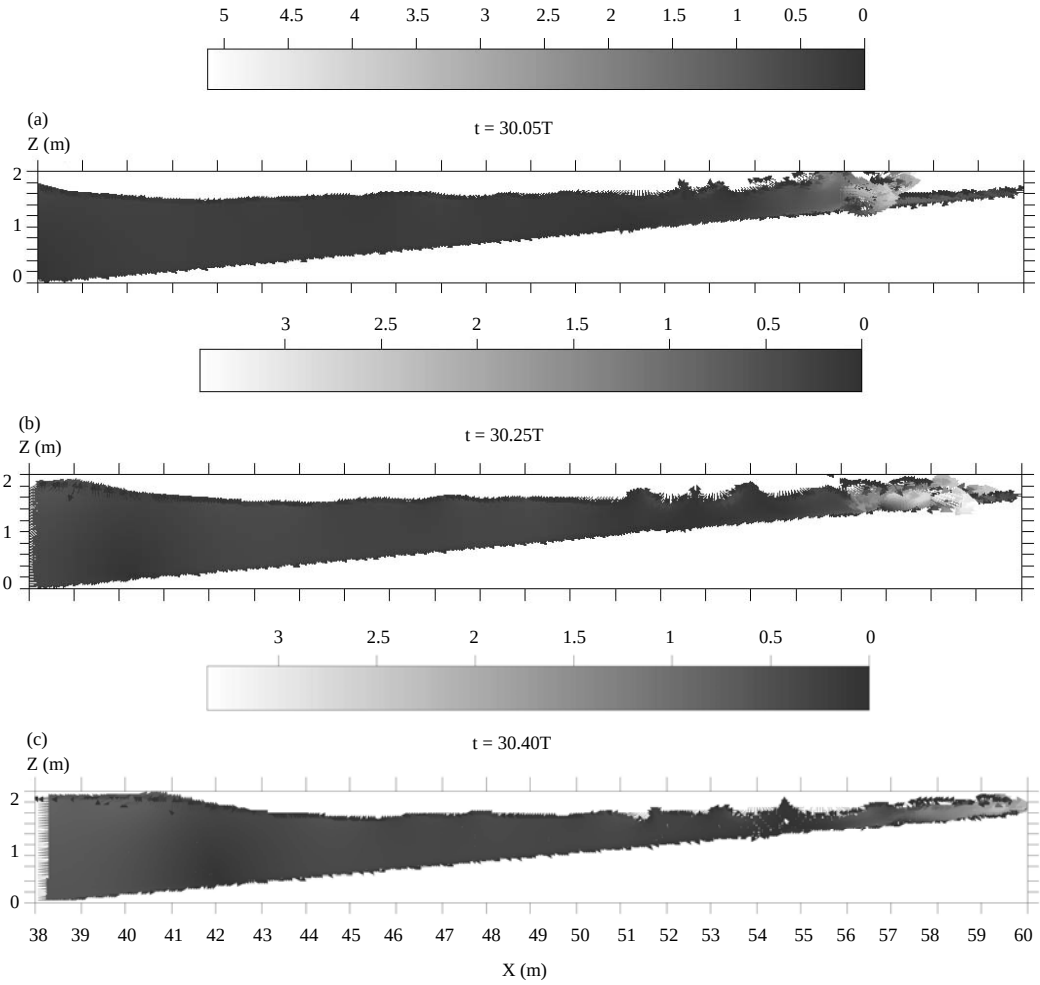

Fig. 5(a-c): $\sqrt{2k}$ field (T = 4.00 s, H_i = 0.40 m) for (a) t = 30.05T, (b) 30.25T and (c) 30.40T

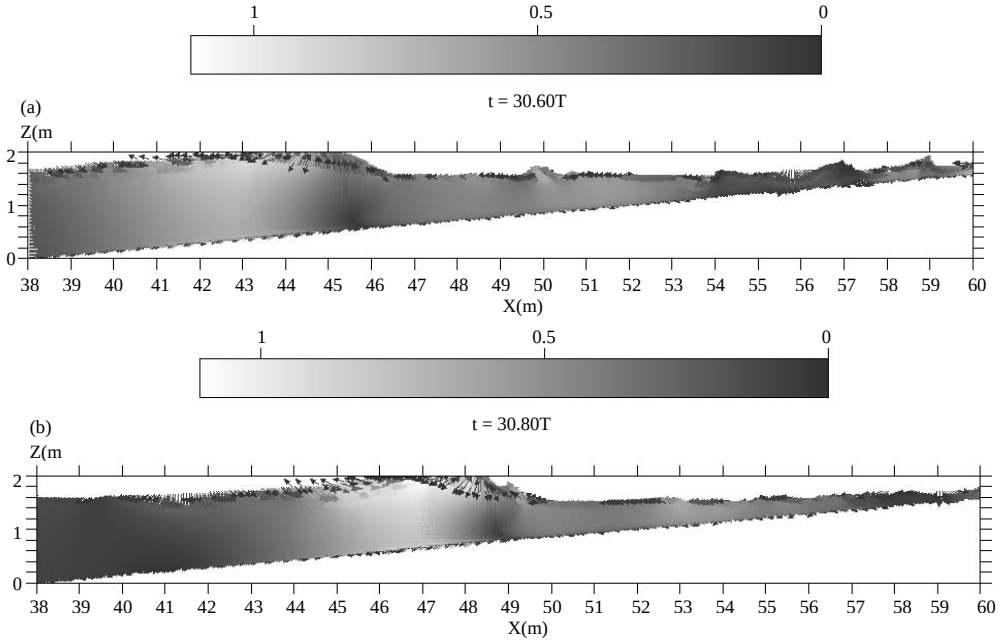

Fig. 6(a-c): Continue

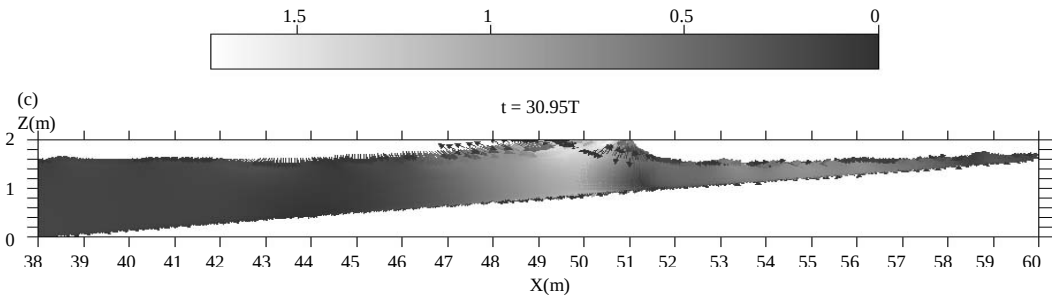

Fig. 6: $\sqrt{2k}$ field (T = 4.00 s, H_i = 0.40 m) for (a) t = 30.60T, (b) 30.80T and (c) 30.95T

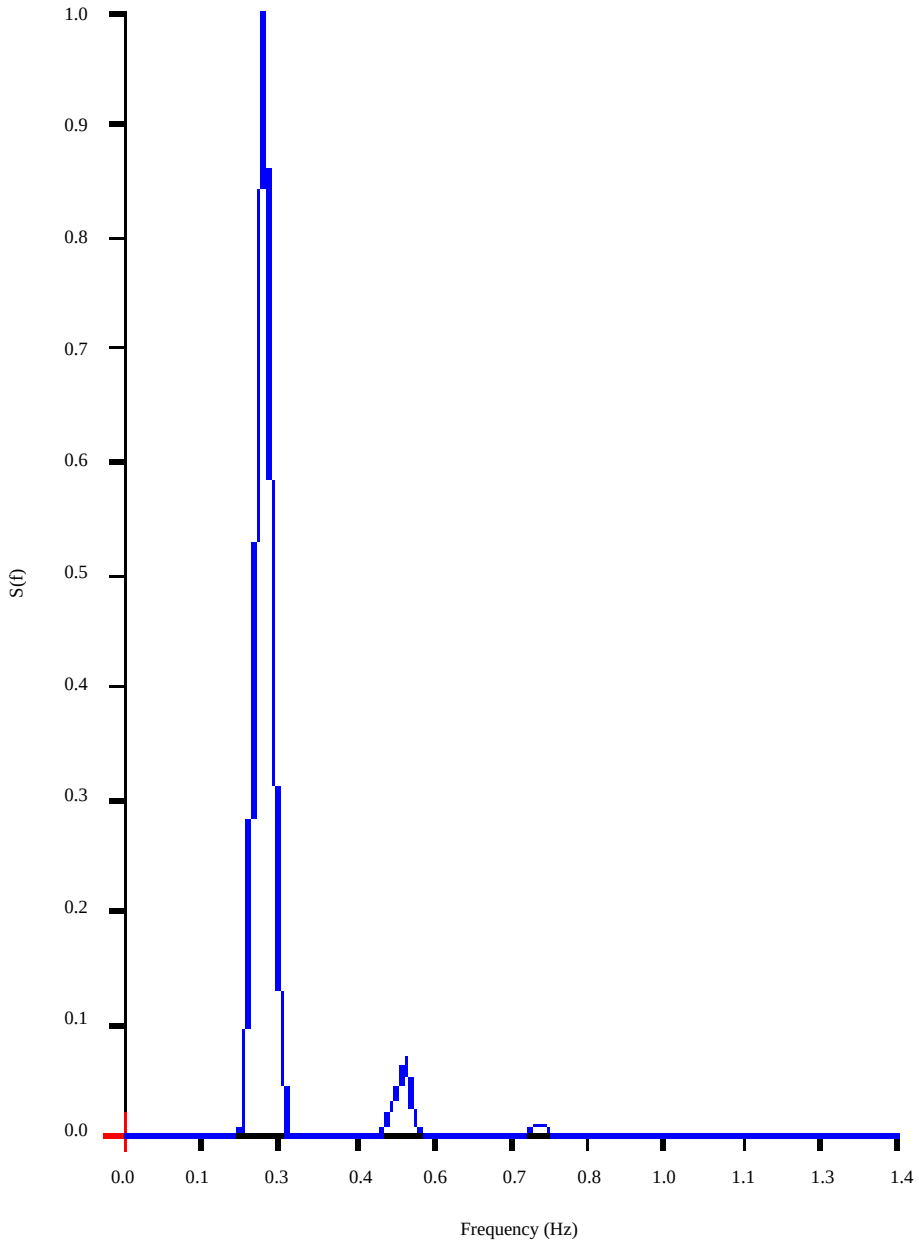

Fig. 7: Wave spectrum-regular waves (T = 4.00 s, H_i = 0.40 m) in WG 1

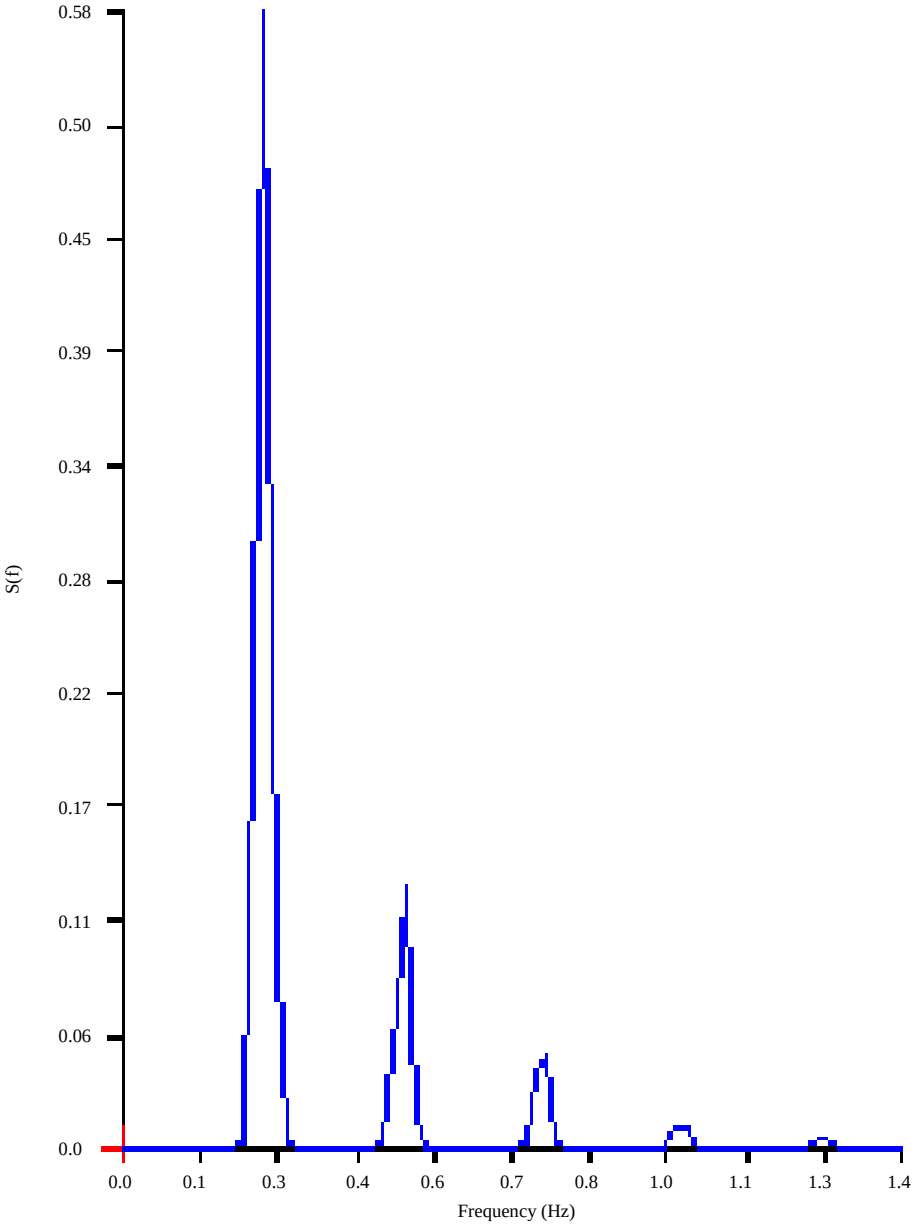

Fig. 8: Wave spectrum-regular waves (T = 4.00 s, H_i = 0.40 m) in WG 2

dissipation occurs at the high-frequency tail (Kolmogorov scale) and energy can be definitely transferred and subsequently absorbed at higher frequencies than the wave harmonics. This is the mechanism that Dimakopoulos and Dimas[25] exploited to model spilling wave breaking in the surf zone using a tailored LES approach.

CONCLUSION

The numerical and experimental simulations covered a range of incident wave conditions covering plunging waves.

According to the analysis of this study, the following conclusions are drawn:

- During wave breaking, the velocity of fluid particles at the wavefront and the region near the free surface precedes the wave speed
- Generally, the wave breaking is well described by the flow model and the turbulence characteristics can be simulated well in time and space by using the k-ϵ model
- Velocity has its maximum value at the upper part, where the surface roller occurs, very close to the free surface, under the wave crest

- The numerical results show the maximum turbulent kinetic energy and dissipation rate are located below the wave crest and near the free surface at breaking time
- Significant non-linear interactions occur in the surf zone and some energy is transferred from the fundamental wave frequency to higher harmonics
- A significant portion of turbulence dissipation occurs at the high-frequency tail (Kolmogorov scale) and energy can be definitely transferred and subsequently absorbed at higher frequencies than the wave harmonics

SIGNIFICANCE STATEMENT

This study provides useful insights to wave breaking and energy transfer mechanism in the surf zone. This study help the researchers to uncover the critical areas of wave breaking induced longshore currents and wave setup. This study discovers the possible synergistic effect of wave breaking and energy transfer mechanism in the surf zone, that can be beneficial for beach morphology, sediment transport and wave energy dissipation.

REFERENCES

1. Hu, K., C.G. Mingham and D.M. Causon, 2000. Numerical simulation of wave overtopping of coastal structures using the non-linear shallow water equations. Coastal Eng., 41: 433-465.
2. Karambas, T.V. and N.P. Tozer, 2003. Breaking waves in the surf and swash zone. J. Coastal Res., 19: 514-528.
3. Lin, P. and P.L.F. Liu, 1998. A numerical study of breaking waves in the surf zone. J. Fluid Mech., 359: 239-264.
4. Ozdemir, C.E., T.J. Hsu and S. Balachandar, 2013. Direct numerical simulations of instability and boundary layer turbulence under a solitary wave. J. Fluid Mech., 731: 545-578.
5. Bradford, S.F., 2000. Numerical simulation of surf zone dynamics. J. Waterway Port Coastal Ocean Eng., 126: 1-13.
6. Christensen, E.D., 2008. Large eddy simulation of spilling and plunging breakers. Coastal Eng., 53: 463-485.
7. Zhao, Q., S. Armfield and K. Tanimoto, 2004. Numerical simulation of breaking waves by a multi-scale turbulence model. Coastal Eng., 51: 53-80.
8. Hirt, C.W. and B.D. Nichols, 1981. Volume of Fluid (VOF) method for the dynamics of free boundaries. J. Comput. Phys., 39: 201-225.
9. Hsu, T.J., T. Sakakiyama and P.L.F. Liu, 2002. A numerical model for wave motions and turbulence flows in front of a composite breakwater. Coastal Eng., 46: 25-50.
10. Lin, P. and P.L.F. Liu, 1999. Internal wave-maker for Navier-Stokes equations models. J. Waterway Port Coastal Ocean Eng., 125: 207-215.
11. Israeli, M. and S.A. Orszag, 1981. Approximation of radiation boundary conditions. J. Comput. Phys., 41: 115-135.
12. Chorin, A.J., 1968. Numerical solution of the Navier-Stokes equations. Math. Comput., 22: 745-762.
13. Losada, I.J., M.A. Losada and A. Martin, 1995. Experimental study of wave-induced flow in a porous structure. Coastal Eng., 26: 77-98.
14. Van Gent, M.R.A., 1994. The modelling of wave action on and in coastal structures. Coastal Eng., 22: 311-339.
15. Ting, F.C.K. and J.T. Kirby, 1995. Dynamics of surf-zone turbulence in a strong plunging breaker. Coastal Eng., 24: 177-204.
16. Sou, I.M. and H. Yeh, 2011. Laboratory study of the cross shore flow structure in the surf and swash zones. J. Geophys. Res.: Oceans, Vol. 116. 10.1029/2010JC006700.
17. Sumer, B.M., H.A.A. Guner, N.M. Hansen, D.R. Fuhrman and J. Fredsoe, 2013. Laboratory observations of flow and sediment transport induced by plunging regular waves. J. Geophys. Res.: Oceans, 118: 6161-6182.
18. Smit, P., M. Zijlema and G. Stelling, 2013. Depth-induced wave breaking in a non-hydrostatic, near-shore wave model. Coastal Eng., 76: 1-16.
19. Lin, T.C., H.L. Wu, S.M. Lo, S.C. Hsia and H.H. Hwung, 2015. Flow characteristics of spilling and plunging breakers in the surf zone. J. Mar. Sci. Technol., 23: 638-648.
20. Ting, F.C.K. and J. Reimnitz, 2015. Volumetric velocity measurements of turbulent coherent structures induced by plunging regular waves. Coastal Eng., 104: 93-112.
21. Watanabe, Y., H. Saeki and R.J. Hosking, 2005. Three-dimensional vortex structures under breaking waves. J. Fluid Mech., 545: 291-328.
22. Farahani, R.J. and R.A. Dalrymple, 2014. Three-dimensional reversed horseshoe vortex structures under broken solitary waves. Coastal Eng., 91: 261-279.
23. Lubin, P. and S. Glockner, 2015. Numerical simulations of three-dimensional plunging breaking waves: Generation and evolution of aerated vortex filaments. J. Fluid Mech., 767: 364-393.
24. Sou, I.M., E.A. Cowen and L.F. Liu, 2010. Evolution of the turbulence structure in the surf and swash zones. J. Fluid Mech., 644: 193-216.
25. Dimakopoulos, A.S. and A.A. Dimas, 2011. Large-wave simulation of three-dimensional, cross-shore and oblique, spilling breaking on constant slope beach. Coastal Eng., 58: 790-801.

26. Lakehal, D. and P. Liovic, 2011. Turbulence structure and interaction with steep breaking waves. J. Fluid Mech., 674: 522-577.
27. Grasso, F., B. Castelle and B.G. Ruessink, 2012. Turbulence dissipation under breaking waves and bores in a natural surf zone. Continental Shelf Res., 43: 133-141.
28. Ting, F.C.K., 2013. Laboratory measurements of large-scale near-bed turbulent flow structures under plunging regular waves. Coastal Eng., 77: 120-139.
29. Zhou, Z., J. Sangermano, T.J. Hsu and F.C.K. Ting, 2014. A numerical investigation of wave-breaking-induced turbulent coherent structure under a solitary wave. J. Geophys. Res.: Oceans, 119: 6952-6973.